Solid Freeform Fabrication 2016: Proceedings of the 27th Annual International Solid Freeform Fabrication Symposium – An Additive Manufacturing Conference
Reviewed Paper

In-Process Monitoring of Cross Contamination in Laser Powder Bed Fusion (L-PBF) Additive Manufacturing (AM)

M. Jamshidinia, P. Boulware, J. Marchal, H. Mendoza, L. Cronley, S. Kelly, S. Newhouse
EWI
1250 Arthur E Adams Dr., Columbus, OH 43221

Abstract

Cross contamination in laser powder bed fusion (L-PBF) Additive Manufacturing (AM) could locally change the chemical composition and stress distribution in a component. It also could result in the formation of flaws, and consequently lower the mechanical performance of a component. In this study, the in-process monitoring and detection of cross contamination was investigated in L-PBF process, also known as direct metal laser sintering (DMLS). A setup was designed and fabricated at EWI, where contaminant materials could be introduced on the powder bed without interrupting the fabrication process or breaking the chamber environment. Tungsten particles were used as the contaminant material, in the matrix of Inconel 625. Six levels of contamination were calibrated, and were introduced in two static and dynamic modes. Photodetector, spectrometer, and optical camera were used for the data acquisition. One of the sensors showed the most promising results. X-ray computed tomography (CT) and optical microscopy were used to validate data collected by the sensors.

Keywords: cross contamination, in-process monitoring, spectrometer, photodetector, laser powder bed fusion (L-PBF)

Introduction

The layer-by-layer fabrication of metallic components in laser powder bed fusion (L-PBF) processes occurs as a result of interactions between a high power laser beam and metallic powder particles. Several studies have been done on the in-process monitoring of PBF processes. G. Zenzinger et al [2015] used a high-resolution camera system to obtain thermal images from the L-PBF process. A three-dimensional (3D) digital map was prepared from the structural irregularities and structural disorder detected by the optical tomography (OT) method. The 3D map was correlated to mechanical performance and failure analysis of specimens. T. Furumoto et al. [2012] used a high speed video camera to investigate the melting and solidification of a ferrous alloy during the L-PBF process. The shape of molten pool as well as the powder scattering influenced by process parameters was visualized. J. P. Kruth et al [2007] used a photodetector and a complementary metal–oxide–semiconductor (CMOS) to monitor and control the size of molten pool. Some coupons with overhanging features were produced with and without the feedback control system. Results showed that both sensors can be integrated in a feedback control system and the melt pool area can be controlled. S. Price et al. [2013] used a near infrared thermal imager for temperature measurements in the electron beam powder bed fusion (EB-PBF) of Ti-6Al-4V. The influence of overhanging features on the size of the molten pool was analyzed at various build heights. B. Foster et al. [2015] used a high-resolution DSLR camera to collect images under oblique illuminations of fused and pre-placed powder layers. Various types of build defects were detected. Also, a three dimensional (3D) reconstruction of a

fabricated part and potential defects was produced using the high exposure optical images. S. Kleszczynsk et al. [2012] used a high-resolution imaging camera to detect errors caused by predefined process irregularities during the L-PBF of Inconel 625. A monochrome charge coupled device (CCD) was sued for this purpose. The same camera was also used to collect data from a cylinder produced with contaminated powders. Results showed a distinguishable difference between the clean and contaminated cylinders. However, the CCD camera did not provide any additional data about the level of contamination.

So far, a limited study has been conducted on the monitoring and detection of cross contamination during the PBF process. In this study, the monitoring and detection of cross contamination were investigated, where the main focus was to provide an experimental and qualitative comparison between the collected data from three sensors, and develop a relationship between the data and the contamination levels. The quantitative analysis of data such as correlating a signal characteristics to contamination levels and contaminant materials will be conducted in the future study.

Design of Experiment

Materials

In this study, a rectangular specimen with a 10×10×15.20-mm dimension was fabricated with Inconel 625. Tungsten powder was the contaminant material to be deposited in between the Inconel 625 layers. A carbon steel plate was sued as the build platform. All powders used in the contamination study were virgin powders.

The Cross Contamination Setup

A setup was designed and fabricated by EWI, for the deposition of precise amount of contamination at each desired step. To minimize the possibility of undesired powder deposition during the fabrication process, the setup was tested for powder leakage. The entire platform under the contamination setup, including dispenser, build plate, and collector was covered. The test was conducted by executing the powder deposition for 100 times. Not a detectable amount of powder was leaked from the powder container on the build platform and collector.

Deposition Calibration

Figure 1 shows the six levels of contamination used for tungsten respectively. There was a 0.5-mm gap between the contamination setup nozzle (on the bottom surface) and the powder bed top surface.

The contamination levels were categorized in two groups. In the first group containing L1, L2, and L3, the contaminant powder was deposited while the recoater was stopped (static category). As a result, a spot-shaped profile of contaminant powder was formed. In the second category (L4, L5, and L6), the contaminant powders were deposited, while the recoater was moving (dynamic category). So, the contaminant powders were spread as an

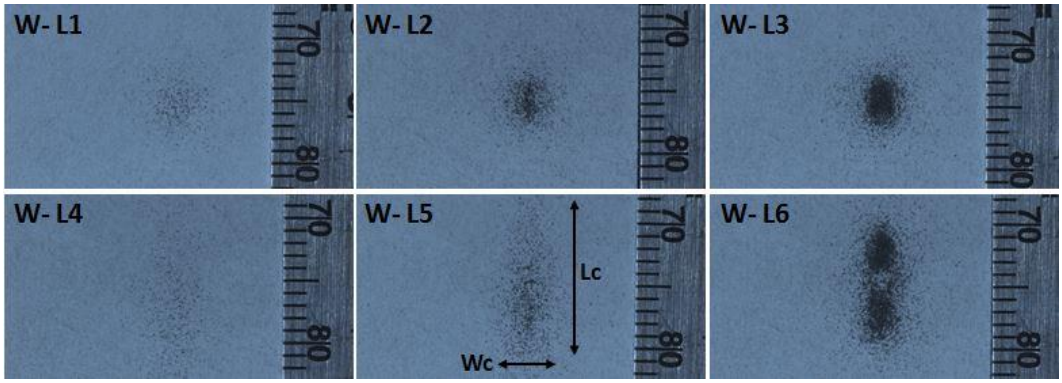

Figure 1. The six levels of contamination deposition for tungsten. Lc and Wc refer to the length and width of a contamination profile.

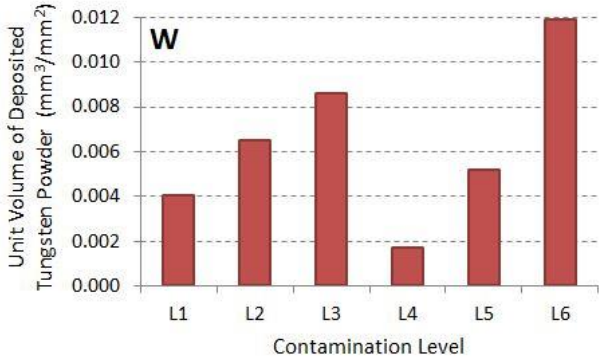

Figure 2. The unit volumes of deposited powders for the six contamination levels for the tungsten (W) powder. L1 to L3 correspond to the static powder deposition. L4 to L6 correspond to the dynamic powder deposition.

elongated line and formed a linear profile on the powder bed. Figure 2 plotted the deposited unit volumes of powder corresponding to the contamination levels.

Build Layout

Table 1 shows the build layout used for the contamination study. The contaminant powder was deposited on a single layer, while 19 layers of baseline parameters were deposited below and above it. Baseline parameters refer to layers of Inconel 625 that were produced without the introduction of contaminant powders. In order to investigate repeatability of data acquisition, the whole set of six contamination levels was repeated three times, consecutively.
Data acquisition was conducted for a total of 10 layers per each contamination layer. Two layer before the contamination, the contamination layer, and seven layers after the contamination were recorded. It should be noted that the labeling of layers on data acquisition data was different than the actual layers numbering.

Table 1. the build layout for the contamination study. The contamination set of L1 to L6 was deposited three times, and was followed by the cover layers.

Contamination Set #	Base Line (BL) / Contamination Layer (Ln, n= 1 to 6)	Start Layer	End Layer	Start Height (mm)	End Height (mm)
Contamination Layers (×3 iterations)	BL	1	19	0.04	0.76
	L1	20	20	0.80	0.80
	BL	21	39	0.84	1.56
	L2	40	40	1.60	1.60
	BL	41	59	1.64	2.36
	L3	60	60	2.40	2.40
	BL	61	79	2.44	3.16
	L4	80	80	3.20	3.20
	BL	81	99	3.24	3.96
	L5	100	100	4.00	4.00
	BL	101	119	4.04	4.76
	L6	120	120	4.80	4.80
Cover Layers	BL	361	380	14.44	15.20

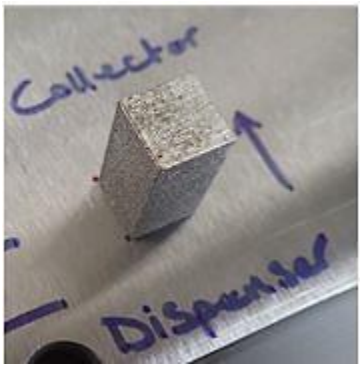

Figure 3. A rectangular specimen made of Inconel 625, containing contamination layers.

Figure 3 shows the rectangular specimen made of Inconel 625, with embedded layers of contamination. Optimum process parameters were developed for the fabrication of Inconel 625 in EWI's test bed.

Data Acquisition

Photodetector, spectrometer, and optical camera were used for the data acquisition. An Ocean Optics HR2000+ sensor was used as the spectrometer. The detection range was 200 to 1100 nm, with an exposure set at 1 ms (frequency of 1000 Hz). The photodetector was a PDA36A sensor from Thor Labs, with a detection range was 350 to 1100 nm. The gain was set at

40dB. Also the signal amplification was tuned to maximize the signal without saturation. A Flea3 optical camera from Point Grey was used to record snapshots of the powder bed top surface after the deposition of the contaminant powders as well as after the fusion by laser. The camera had an 8.8 mega pixel resolution, with a field of view of 1.0 × 0.58 in, and was able to capture one frame per second. Both of the spectrometer and photodetector were installed on the optical table and aligned with the on-axis signal.

Figure 4 shows the results of data acquired from a tungsten-contamination build. The two graphs on the top and the middle plotted data collected by the spectrometer and photodetector, respectively. The two images shown in the bottom row of each contamination level were taken after the deposition of the contaminant powder and after the fusion by laser. The darker profiles on the optical images refer to the tungsten powder spread over the powder bed.

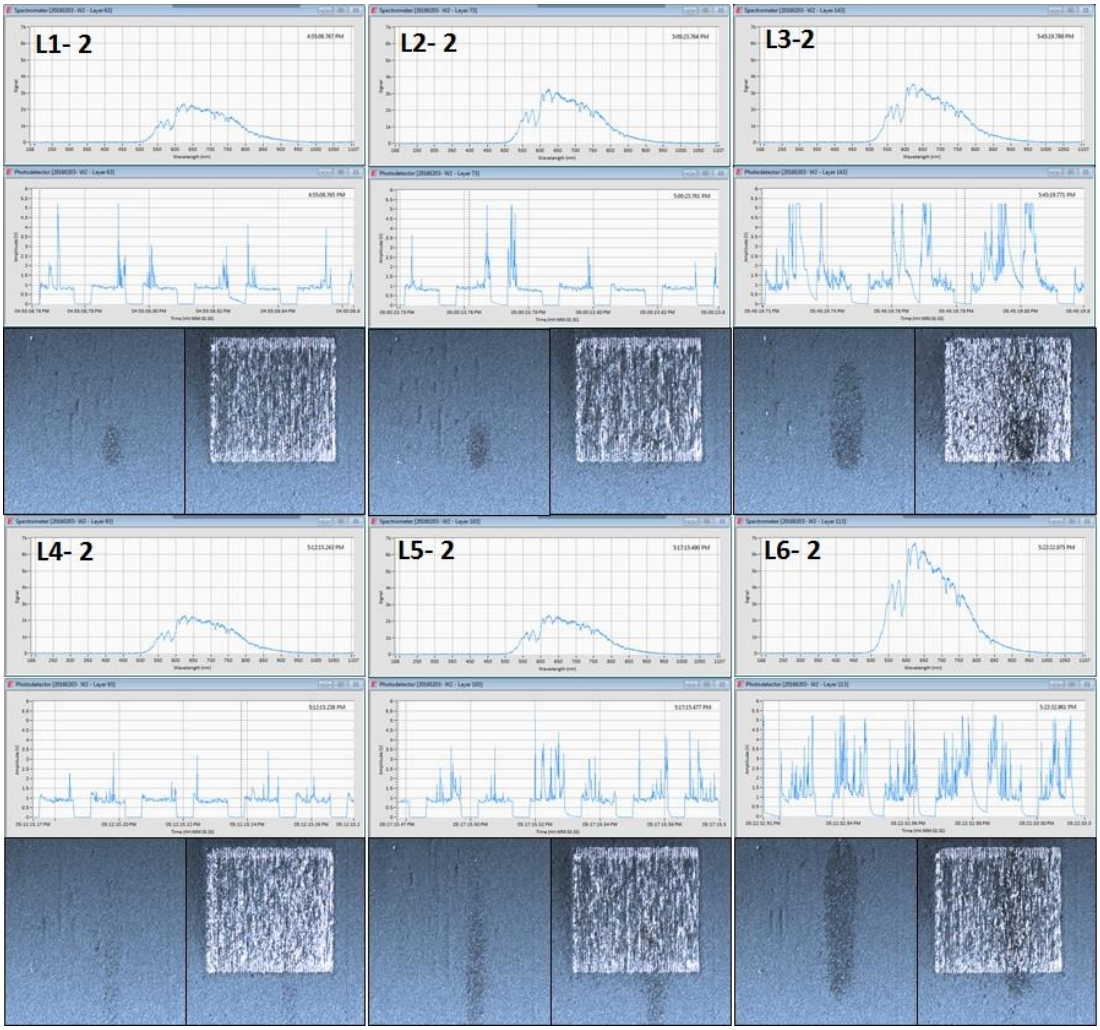

Figure 4. Results of data acquisition using spectrometer (top), photodetector (middle), and optical camera (bottom) during the deposition of tungsten contaminants. L1 through L6 refers to the six levels of contamination. Also, 2 refers to the second iteration of contamination deposition.

Spectrometer

Regardless of the contamination level, the data collected by the spectrometer showed signals (peaks) at identical wavelengths. However, the signals had different intensities (strengths). A general relationship could be established between the contamination levels and the maximum signal strengths. Spectrometer detected a stronger signal with an increase in the compactness (unit volume) of a contamination level (Figure 4). For example, L6 showed a signal with the maximum strength. However, the contamination levels with low unit volumes, such as L1, L4, and L5 did not show signals with distinguishable differences. It could be related to the limited capability of the spectrometer in detecting contaminations with low unit volumes. Therefore, only the tungsten contamination levels with a unit volume of 0.006 mm^3/mm^2 or higher could be distinguishably detected by the spectrometer used in this study.

It should be noted that the spectrometer used in this study had a data acquisition frequency of 1000 Hz. A spectrometer with a higher frequency might be able to capture more accurate data from different contamination levels that could make collected data more distinguishable.

Optical camera

According to Figure 4, all contamination levels except L1 and L4 showed clearly detectable discolorations on the top surface of the specimen after the deposition of contaminant powder. In some cases such as L3 and L6, the discoloration was detectable even after the fusion of the powder bed. Because the unit volumes deposited in L1 and L4 were low, not enough contrast were formed between the contaminated zone and rest of the top surface. The optical camera used in this study was able to detect the tungsten contamination levels with a unit volume of 0.005mm^3/mm^2 and higher.

It should be noted that the development of an improved illumination system, as well as the synchronization of the optical camera with an image analysis code would improve the quality and reliability of data captured by the optical camera.

Photodetector

There was a strong relationship between the contamination levels and the data collected by the photodetector. Figure 5 illustrates the characteristics of signals generated by the photodetector. The horizontal axis shows the data acquisition time. Each set of data is the representative of one hatch line (Figure 5-a). Depending on unit volume deposited on the powder bed as well as the profile of the deposited contaminant powder, a single peak (Figure 5-b) or multiple peaks (Figure 5-c) were recorded. Figure 5-d shows the profile of the deposited contaminant powder for the contamination level of L3. Lc and Wc refer to the length and width of the deposition profile, respectively. The dashed-black arrow shows the recoating direction.

Figure 6 illustrates the contamination profiles with their associated photodetector data. Any of the images consisted of data collected from six consecutive hatches and was equivalent to

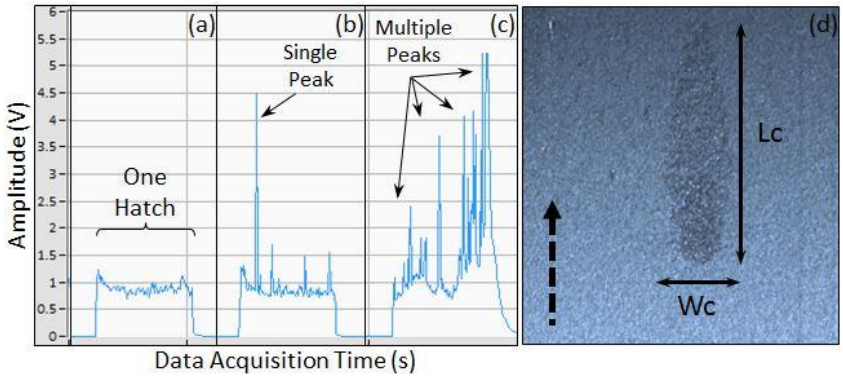

Figure 5. The characteristics of signals generated by the photodetector, a) each data set was a representative of one hatch line. B) Single peak, c) Multiple peaks, d) The distribution of tungsten powder on the powder bed, where Lc and Wc refer to the length and width of the contaminant powder profile, respectively. The black dashed line shows the recoating direction.

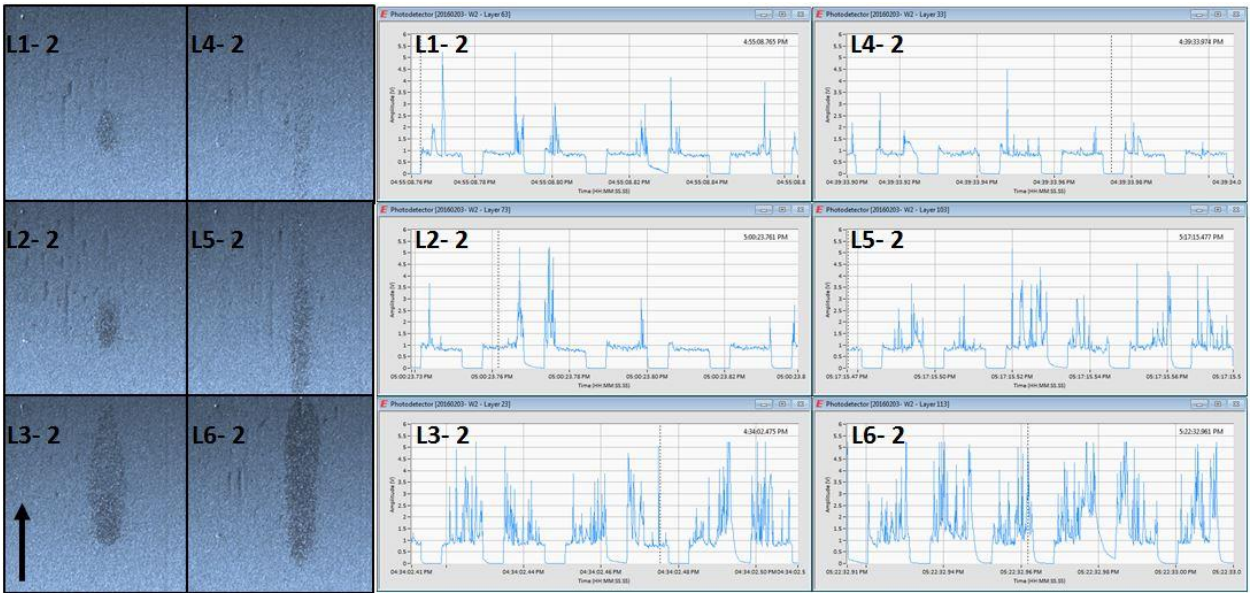

Figure 6. Correlation between the contamination profile and the photodetector data. The number and strength of signals detected by the photodetector varied with contamination levels. The black arrow shows the laser scanning direction as well as the recoating direction.

0.1 seconds of the scanning process. The data collected from the six contamination levels were different in the following items:

- Number of peaks per hatch
- Intensity of the peaks
- Number of hatches with high intensity peaks

The black arrow in Figure 6 shows the laser scanning direction as well as the recoating direction. At a contamination level with a longer length (Lc), the contaminant powder was exposed to the laser beam for a longer period of time. As a result, multiple peaks were generated and recorded by the photodetector. Therefore, the presence of multiple peaks per hatch at L3-2 and L6-2 could be related to the elongated length of the deposition profile.

The intensity of a peak could be related to deviation of the molten pool from a default condition. The application of a contaminant powder profile with a higher compactness (or a higher unit volume) results in a larger deviation from a default condition. Therefore, even though both of the L5-2 and L6-2 contamination levels had an elongated deposition profile and showed multiple peaks per hatch, L6-2 had stronger peaks were due to its higher compactness (unit volume) of contaminant powder.

More hatches with strong peaks could be recorded if a contamination profile had a wide contamination width (Wc). However, a high compactness was also necessary for the formation of multiple hatches with high intensity peaks.

Detectability after the contamination

This section investigated the possibility of detecting tungsten contaminations in consecutive layers. Because the photodetector showed the most promising data so far, data collected by the photodetector were analyzed for this purpose. Figure 7 compares the photodetector data collected from four consecutive layers of each contamination levels. The first set of data on the top corresponds to the contamination layers, where a contaminant powder was deposited on it. This layer was identified by n. Layer n+3, at the bottom row, represents the third layer on top of a contamination layer. As shown, almost all contamination levels still showed some distinguishable signals on the second layer (n+1); however the signals were weaker than those on the first layer. However, by the deposition of two more layers, most of the initially detected signals disappeared. Even at L3, with a high unit volume deposited on the powder bed, almost all signals were faded out on layer n+3. L5 and L6 were the only two contamination levels that still showed one signal on layer n+3. These results suggest that a contamination with tungsten, even at very high levels, could only be detected for up to three layers (120 μm) on top of where the contaminant powders were introduced. It has to be noted that none of the contamination levels showed any signals on layer n+4.

Post process inspection

Metallurgical analysis

The specimen with embedded tungsten contaminant was sectioned, mounted, and polished, for further metallurgical analysis. An alcohol-based Kalling's etching solution was used for the primary etching. Then specimens were etched using a 10% chromic acid solution at 2.4 volts. Figure 8 shows the low magnification (25X) images of the cross sections. The white arrows indicate the contamination deposition layers. The black arrow indicates the buildup direction. The tungsten particles with a white color could be clearly detected on the matrix of Inconel 625.

Figure 7. Data collected from photodetector from the six levels of contamination with tungsten. Four layers per contamination level are studied.

Figure 8. Low magnification optical images of the specimens contaminated by tungsten. The white arrows indicate the contamination deposition layers. The black arrow indicates the buildup direction.

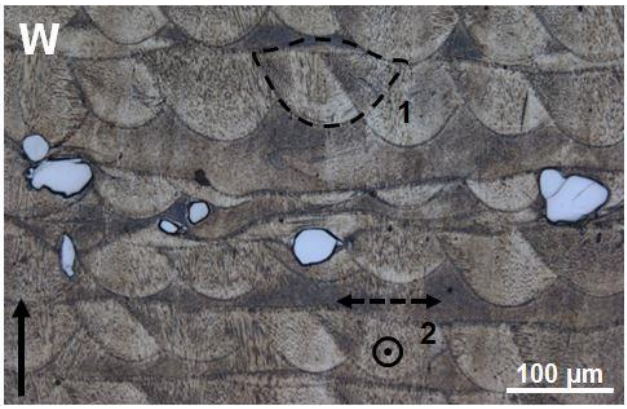

Figure 9. High magnification optical images of the specimens contaminated by tungsten. The white arrows indicate molten pools with distorted appearance. The black arrow indicates the buildup direction.

Figure 9 shows a high magnification image of the contaminated specimen. The solid black arrow indicates the buildup direction. Similar to Figure 8, the white tungsten (W) particles could be observed with a high contrast with the Inconel 625 matrix. These cross sectional images could also provide some additional information about the L-PBF process. The dashed-line (1) indicates the shape of a molten pool, penetrated into the previously deposited layer. Also, the overlaps between tracks could be recognized. However, the layer below the indicated molten pool had a different appearance, with no indications of molten pool profiles. The dashed line and circle (2) shown at the bottom of the tungsten specimen are representative of the hatching directions in the two consecutive layers. When the laser scanning direction is normal to the polishing surface, molten pools are formed normal to the polishing surface and could be observed on etched specimens. Because the hatching direction was rotated 90 degree between

layers, the molten pool of the consecutive layer formed parallel to the polishing surface, and was observed as a long continuous stripe.

X-Ray Computed Tomography (CT)

Metallurgical analysis provided some information about the contaminated specimens. However, it was limited to only one cross section per specimen. To better understand the distribution and melting of contaminant powders, one specimen per contaminant material was inspected using X-Ray Computed Tomography (CT). Figure 10 illustrates the 3D reconstruction of the specimen contaminated with the tungsten powder particles. The three planes represent the three axes of the Cartesian coordinate system. The recoating direction is shown by the black arrow. The vertical cross-sectional views of the reconstructed specimen are presented in Figure 11. The white arrow indicates the recoating (or powder spreading) direction. Seventeen layers of contaminated powders could be detected, while the second layer from the bottom (Level L2) was missing. The missing layer was indicated using the white stars in Figure 11. Figure 11-a shows the cross sectional view normal to the recoating direction. The white-dashed line box indicates the second set of contamination levels, from L1 to L6, embedded in the specimen. The results of the CT confirmed that the minimum and maximum amounts of powder were deposited in L4 and L6, respectively. Figure 11-b provided additional information on the tungsten powder distribution, with a cross-section parallel to the recoating direction. The three contamination levels of L6 were shown to distinguish the three consecutive sets of contamination levels. The contamination levels L4 through L6 had elongated powder tails, due to their dynamic powder deposition system. L1 and L2 with the static powder deposition had the shortest tails of powder. The contamination level L3 was expected to have a short tail, as well. But a long

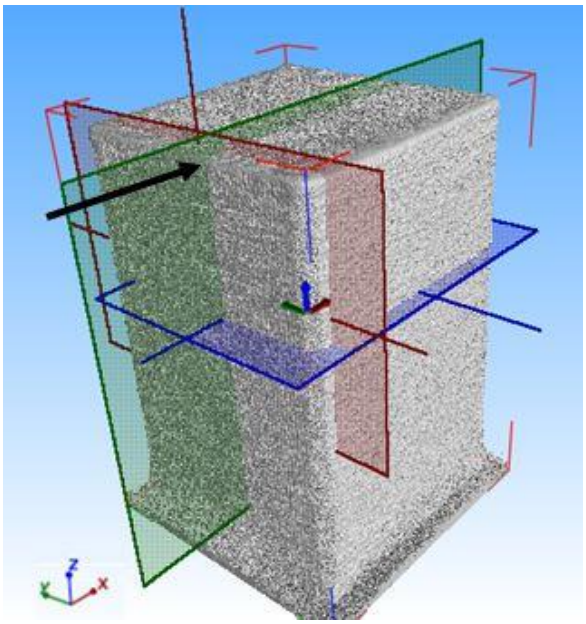

Figure 10. Three-dimensional (3D) reconstruction of the specimen contaminated with tungsten powder particles. The black arrow shows the powder recoating direction.

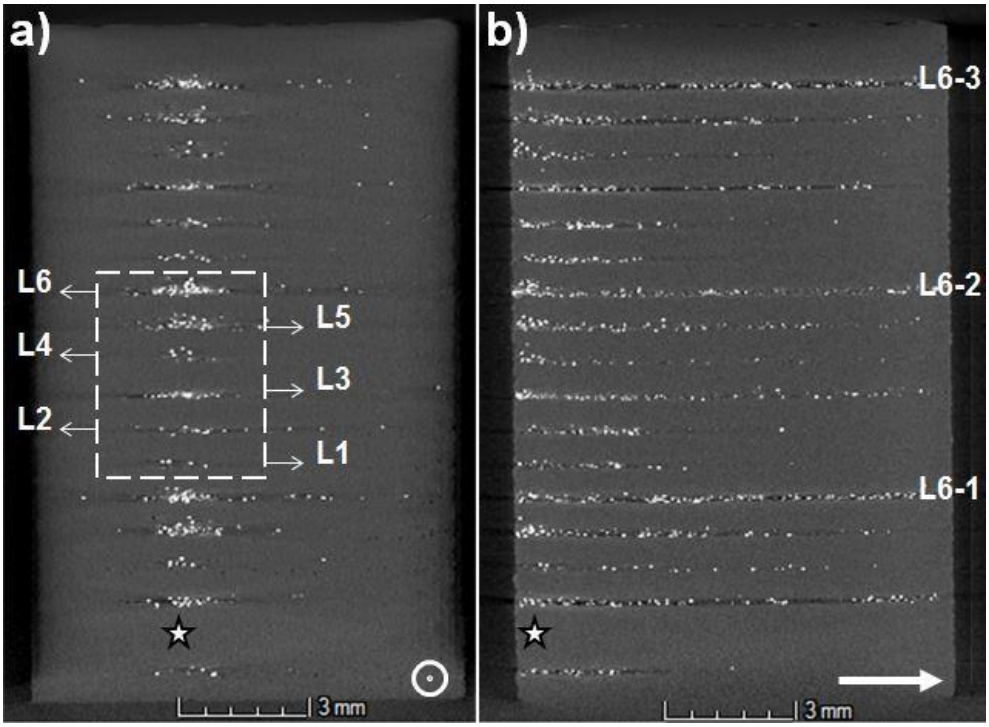

Figure 11. The vertical cross sectional views of the specimen contaminated by the tungsten powder particles, a) cross section normal to the recoating direction, b) cross section along the recoating direction

powder tail was observed on all of the three iterations of L3 levels. The unexpected powder distribution in L3 was attributed to the transfer of contamination between consecutive layers, which will be studied in future works.

Figure 12 illustrated the horizontal view of the tungsten powder distribution in the six contamination levels. There was a noticeable match between the calibration images shown in Figure 1 and the actual distribution inside the specimen.

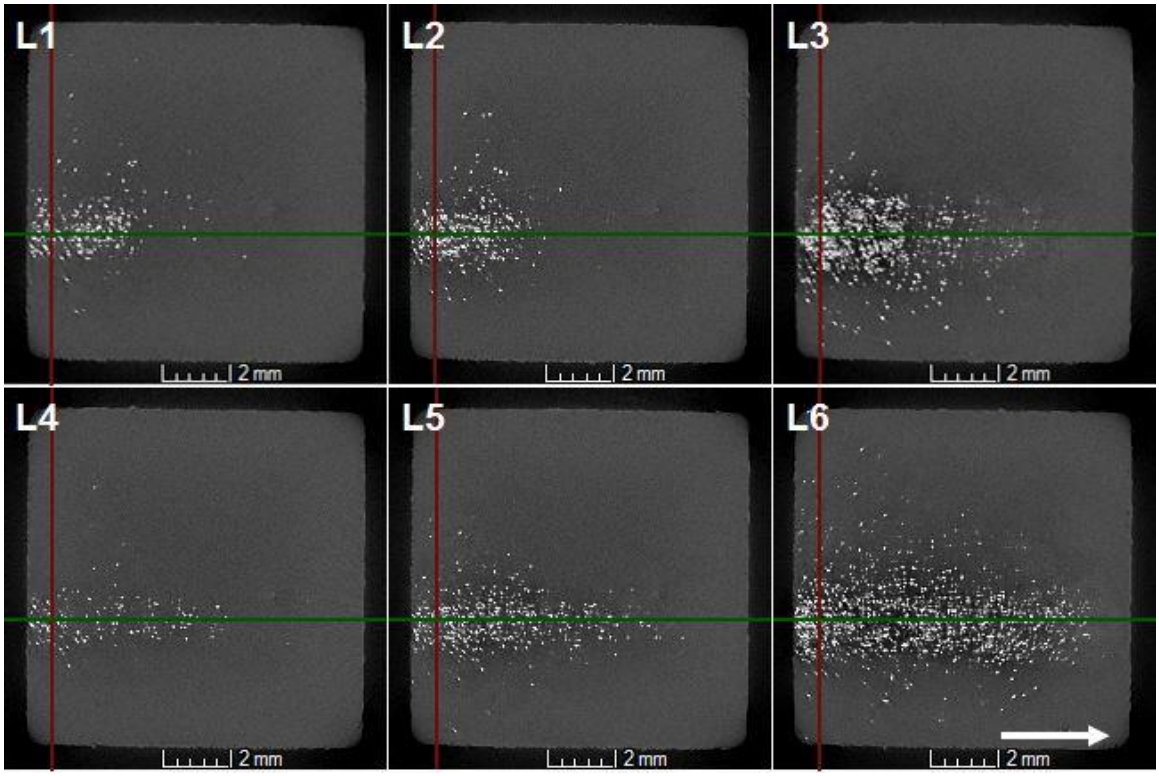

Figure 12. The horizontal cross sectional views of the specimen contaminated with the tungsten powder. Images show the six contamination levels, along the buildup direction (shown by the white arrow).

Conclusion

The cross contamination of Inconel 625 was studied during the L-PBF process. A setup was designed and fabricated by EWI for this purpose. The Tungsten powder was used as the contaminant material. Three sensors including spectrometer, photodetector, and optical camera were used to monitor the process. The contaminated specimens were studied metallurgically. Also, X-ray CT was used to reconstruct the 3D model of the contaminated specimens and investigate the distribution of contaminant powders.

The results of this study could be summarized as following:

1. Among the current sensors used in this study, photodetector was the most promising sensor that detected all of the contamination levels of tungsten. Spectrometer and optical camera were able to detect the contamination levels with a unit volume equal to or higher than 0.006 mm^3/mm^2 and 0.005mm^3/mm^2, respectively.
2. Even at the highest level of tungsten deposition, a contamination could be detected for up to three layers (120 µm) on top of where the contaminant powders were initially introduced.

3. The size of area contaminated area became larger in consecutive layers, due to the transfer of unfused particles along the recoating direction, as well as the buildup direction.
4. The minimal dilution of the tungsten particles in the matrix could be explained by considering the melting temperatures of materials used in this study. The process parameters were optimized for the L-PBF of Inconel 625, which was too low for the melting of tungsten.

Future Study

The detection of contamination in L-PBF processes could be further developed through the implementation of the following items:

1. Detectability of other materials will be investigated.
2. The quantitative analysis of data including identifying types of contaminating materials will be conducted in the future study. The application of a spectrometer with a higher data acquisition frequency could help in analyzing spectra and elements.
3. Application of the following sensors could provide additional information from the molten pool:
    a. High speed charge coupled device (CCD) camera
    b. Local thermal sensor
    c. Global thermal sensor (IR camera)
4. Development of an improved illumination system, as well as the synchronization of the optical camera with an image analysis code that could improve the quality and reliability of data captured by the optical camera.

Reference

Foster BK, Reutzel EW, Nassar AR, Hall BT, Brown SW, Dickman CJ. Optical, layerwise monitoring of powder bed fusion, In Proceedings of the Solid Freeform Fabrication Symposium. 2015, pp. 295-307.

Furumoto T, Alkahari MR, Ueda T, Aziz MS, Hosokawa A. Monitoring of laser consolidation process of metal powder with high speed video camera. Physics Procedia, 2012,39, pp.760-6.
Kleszczynski S, Zur Jacobsmühlen J, Sehrt JT, Witt G. Error detection in laser beam melting systems by high resolution imaging. In Proceedings of the Solid Freeform Fabrication Symposium. 2012.

Kong F, Ma J, Carlson B, Kovacevic R. Real-time monitoring of laser welding of galvanized high strength steel in lap joint configuration, Optics and Laser Technology. 2012, 44 (7), pp. 2186-96.

Kruth JP, Mercelis P, Van Vaerenbergh J, Craeghs T. Feedback control of selective laser melting. In Proceedings of the 3rd international conference on advanced research in virtual and rapid prototyping, 2007, pp. 521-527.

Price S, Lydon J, Cooper K, Chou K. Experimental temperature analysis of powder-based electron beam additive manufacturing. In Proceedings of the Solid Freeform Fabrication Symposium. 2013, pp. 162-173.

Zenzinger G, Bamberg J, Ladewig A, Hess T, Henkel B, Satzger W. Process monitoring of additive manufacturing by using optical tomography. In Proceedings of the AIP Conference 2015, 1650 (1), pp. 164-170.